



HAL
open science

Green Synthesis of Sustainable and Cost-Effective TiO₂-SiO₂-Fe₂O₃ Heterojunction Nanocomposites for Rhodamine B Dye Degradation Under Sunlight

Sara Oumenoune Tebbi, Abdeltif Amrane, Reguia Boudraa, Jean-Claude Bollinger, Stefano Salvestrini, Muhammad Imran Kanjal, Ammar Tiri, Lazhar Belkhiri, Maymounah N. Alharthi, Lotfi Mouni

► To cite this version:

Sara Oumenoune Tebbi, Abdeltif Amrane, Reguia Boudraa, Jean-Claude Bollinger, Stefano Salvestrini, et al.. Green Synthesis of Sustainable and Cost-Effective TiO₂-SiO₂-Fe₂O₃ Heterojunction Nanocomposites for Rhodamine B Dye Degradation Under Sunlight. *Water*, 2025, 17 (2), pp.168. 10.3390/w17020168 . hal-04919396

HAL Id: hal-04919396

<https://hal.science/hal-04919396v1>

Submitted on 29 Jan 2025

HAL is a multi-disciplinary open access archive for the deposit and dissemination of scientific research documents, whether they are published or not. The documents may come from teaching and research institutions in France or abroad, or from public or private research centers.







L'archive ouverte pluridisciplinaire **HAL**, est destinée au dépôt et à la diffusion de documents scientifiques de niveau recherche, publiés ou non, émanant des établissements d'enseignement et de recherche français ou étrangers, des laboratoires publics ou privés.



Distributed under a Creative Commons Attribution 4.0 International License

Article

Green Synthesis of Sustainable and Cost-Effective TiO₂-SiO₂-Fe₂O₃ Heterojunction Nanocomposites for Rhodamine B Dye Degradation Under Sunlight

Sara Oumenoune Tebbi ¹, Abdeltif Amrane ¹, Reguia Boudraa ², Jean-Claude Bollinger ³, Stefano Salvestrini ⁴, Muhammad Imran Kanjal ⁵, Ammar Tiri ⁶, Lazhar Belkhiri ⁶, Maymounah N. Alharthi ⁷ and Lotfi Mouni ^{2,*}

¹ Univ Rennes, Ecole Nationale Supérieure de Chimie de Rennes, CNRS, ISCR—UMR 6226, F-35708 Rennes, France; sara-oumenoune.tebbi@ensc-rennes.fr (S.O.T.); abdeltif.amrane@univ-rennes.fr (A.A.)

² Laboratoire de Gestion Et Valorisation Des Ressources Naturelles Et Assurance Qualité, Faculté SNVST, Université de Bouira, Bouira 10000, Algeria; rboudraa@univ-bouira.dz

³ Laboratoire E2Lim (Eau Environnement Limoges), Université de Limoges, 123 Avenue Albert Thomas, 87060 Limoges, France; jean-claude.bollinger@unilim.fr

⁴ Department of Environmental, Biological and Pharmaceutical Sciences and Technologies, University of Campania “Luigi Vanvitelli”, Via Vivaldi 43, 81100 Caserta, Italy; stefano.salvestrini@unicampania.it

⁵ Henan Key Laboratory of Polyoxometalate Chemistry, College of Chemistry and Chemical Engineering, Henan University, Kaifeng 475004, China; mimrankanjal@henu.edu.cn

⁶ Laboratory of Applied Research in Hydraulics, University of Mustapha Ben Boulaid Batna 2, Batna 05000, Algeria; a.tiri@univ-batna2.dz (A.T.); belkhiri.la@gmail.com (L.B.)

⁷ Department of Chemistry, College of Science, Princess Nourah Bint Abdulrahman University, P.O. Box 84428, Riyadh 11671, Saudi Arabia; mnaalharthi@pnu.edu.sa

* Correspondence: l.mouni@univ-bouira.dz

Abstract: TiO₂-SiO₂-Fe₂O₃ heterojunction using the ceramic technique was used in this study to investigate its effectiveness as a photocatalyst for Rhodamine B (RhB) dye degradation. Structural, optical, and morphological characterizations of the synthesized materials were carried out by X-ray diffraction (XRD), photoluminescence analysis (PL), scanning electron microscopy (SEM-EDS), and diffuse reflectance spectroscopy (DRS) to calculate the gap energy. In addition, a degradation rate of around 97% was obtained at a pH of 8, an initial RhB concentration of 10 mg·L⁻¹, a TS-1F semiconductor dosage of 1 g·L⁻¹, and a reaction time of 210 min. The ability of photocatalysis to degrade RhB at different ratios, pH, and with/without H₂O₂ in aqueous media was evaluated under UV light, visible light (250 W), and sunlight. When it comes to the degradation of RhB under visible light (250 W) and sunlight, respectively, the influence of the *n-p* junction showed promising results for the degradation of RhB. In contrast, there was no discernible photocatalytic activity under UV light, which proves that the absorbance switched from UV to visible, demonstrating the decrease in the band gap energy. Additionally, an analysis of the procedure's cost-effectiveness and reusability through an economic study revealed that the synthesized material was interesting in terms of both cost and sustainability.

Keywords: nanoparticles; photocatalytic activity; rhodamine B; heterojunction; TiO₂-Fe₃O₄-SiO₂



Academic Editor: Andrea G. Capodaglio

Received: 19 November 2024

Revised: 20 December 2024

Accepted: 7 January 2025

Published: 10 January 2025

Citation: Tebbi, S.O.; Amrane, A.; Boudraa, R.; Bollinger, J.-C.; Salvestrini, S.; Kanjal, M.I.; Tiri, A.; Belkhiri, L.; Alharthi, M.N.; Mouni, L. Green Synthesis of Sustainable and Cost-Effective TiO₂-SiO₂-Fe₂O₃ Heterojunction Nanocomposites for Rhodamine B Dye Degradation Under Sunlight. *Water* **2025**, *17*, 168. <https://doi.org/10.3390/w17020168>

Copyright: © 2025 by the authors. Licensee MDPI, Basel, Switzerland.

This article is an open access article distributed under the terms and conditions of the Creative Commons Attribution (CC BY) license (<https://creativecommons.org/licenses/by/4.0/>).

1. Introduction

Numerous carcinogenic and poisonous organic dyes are present in industrial effluents, posing a serious risk to human health and the environment. Many wastewater treatment

techniques have been investigated recently, among which the advanced oxidation processes (AOPs) have shown to be successful in degrading contaminants.

Wastewater from the textile industry contains a variety of dyes that, without proper treatment before disposal, become harmful to flora and fauna. Eliminating organic dyes from wastewater is thus a crucial step. These dyes are usually classified depending on their chromophore groups into various classes, including azo, anthraquinone, indigoid, phthalocyanine, sulfur, and triphenylmethane derivatives [1]. It has been estimated that around 7105 tons of 1000 different classes of dyes and pigments are produced every year [1]. Most of these dyes are dangerous; when they are discharged into rivers and streams, they cause structural changes that are harmful to the environment and ecosystems because they severely reduce aquatic life's ability to absorb oxygen and harm aquatic flora and wildlife [2].

Several wastewater treatment processes have been successfully implemented for dye removal, including ozonation and UVC lamp technologies; nevertheless, each of these procedures has drawbacks [3]. Pollutants are transferred between steps of filtration, which calls for regular maintenance, as these techniques consume a tremendous amount of energy. Furthermore, membrane filtration, heterogeneous photocatalysis [4], adsorption [5,6], ultrasonic treatment [7], and coagulation-flocculation [8] were usually used as water purification techniques. Among all these techniques, heterogeneous photocatalysis is an advanced oxidation technique that has become one of the most effective processes for removing persistent pollutants based on the use of the optical properties of semiconductors.

Photocatalysis is based [9,10] on the excitation of a semiconductor by a light source, which generates the migration of electrons e^- from the valence band (BV) to the conduction band (BA). The generated electrons react with water to form hydroxide radicals, which can break down organic molecules into carbon dioxide and water [11].

Of all the materials examined, titanium dioxide (TiO_2) is the most widely used semiconductor in water treatment for its low cost, stability, and non-toxicity. Nevertheless, two drawbacks reduce its application: (i) a large band gap (3.0–3.2 eV), which allows photocatalytic activity only in the ultraviolet, and (ii) rapid electron–hole pairs recombination, which reduces its photocatalytic activity [4]. As a result, numerous attempts have been undertaken to dope the transition metal and nanocomposites in order to increase TiO_2 absorptive capacity to visible light. An alternate method of improving semi-conductors' visible light photocatalytic activity is doping them with non-metal elements.

The TiO_2 - SiO_2 mixture considerably improves the adsorption phenomenon on the silica surface, which in turn improves the photocatalytic properties of the composite compared with TiO_2 alone [12]. According to Babyszko et al. (2022), the addition of SiO_2 prevents TiO_2 from crystallizing. Additionally, compared to TiO_2 (18 nm), Ramamoorthy et al. (2016) reported a decrease in the crystallite size of TiO_2 - SiO_2 (9–12 nm) [13,14]. The distance that photogenerated electrons and holes can move to the regions of activity on the TiO_2 surface is shortened by the reduction in size of the TiO_2 - SiO_2 particles. TiO_2 - SiO_2 is a more effective photocatalyst than TiO_2 because it enhances the efficiency of the electron–hole redox process while concurrently lowering the recombination rate of photoinduced electrons and holes.

In addition, the incorporation of SiO_2 increases the amount of water and hydroxyl groups retained on the surface, which improves the hydrophilic and photocatalytic performances [15–17]. However, the combination of TiO_2 with SiO_2 does not improve the visible photocatalytic activity of TiO_2 ; in order to increase it in the visible range, it is important to incorporate a third material, which allows for the absorption of photons of sunlight [18].

Researchers' attention has recently been drawn to the production of Fe_2O_3 - TiO_2 -based nanocomposite photocatalysts because of its effectiveness in eliminating impurities

from water [19,20]. For $\text{Fe}_2\text{O}_3\text{-TiO}_2$ materials fabrication, various chemical and physical methods, including the sol–gel process, sonochemical method, electrochemical deposition, evaporation-induced self-assembly, atomic layer deposition (ALD), mechanochemical synthesis, hydrothermal preparation techniques [21], ultrasonic-assisted co-precipitation method, ethanol-assisted hydrothermal method, and thermal decomposition method [19] can be used. In a previously published paper, the synthesis of $\text{Fe}_2\text{O}_3\text{-TiO}_2$ composite nanotubes was studied obtaining an ideal dosage of 5.9 at% [22]. Furthermore, $\text{Fe}_2\text{O}_3\text{-TiO}_2$ nanoparticles (NPs), when exposed to sunlight, demonstrated more photocatalytic activity for the purification of water than TiO_2 . Moreover, iron increases the absorption of visible light by adding new levels to TiO_2 's band gap [23]. Iron serves as an electron trap and facilitates the separation of electrons and holes produced by photolysis. Iron is also an inexpensive, non-toxic, and readily available metal element for real-world applications [23,24].

The aim of this work was to investigate, for the first time, the photodegradation efficiency of Rhodamine B (RhB) over the heterojunction of $\text{TiO}_2\text{-SiO}_2\text{-Fe}_2\text{O}_3$ composites at different operating conditions under visible and solar light in order to optimize the degradation performance of the catalyst against RhB. In addition, its solid-state physico-chemical, phase structure, microstructure, and optical properties were investigated using a variety of analytical methods, including scanning electron microscopy (SEM), Fourier transform infrared (FT-IR) spectroscopy, and X-ray diffraction (XRD). Moreover, the cost and reusability of this catalyst were studied in detail in order to use it on an industrial scale.

2. Material and Methods

2.1. Chemicals

High purity (analytical grade) reagents were used in this study, including iron (III) oxide (Fe_2O_3 , 99.9%, $\text{MW} = 159.69 \text{ g mol}^{-1}$), titanium oxide (TiO_2 , 99.5%, $\text{MW} = 79.89 \text{ g mol}^{-1}$), Rhodamine B ($479.02 \text{ g mol}^{-1}$), SiO_2 (60.08 g mol^{-1}), NaOH (39.99 g mol^{-1}), HCl (36.47 g mol^{-1}), and H_2O_2 (34.01 g mol^{-1}), which were obtained from Sigma Aldrich (Darmstadt, Germany). All materials were used without any additional purification steps. Deionized water (DI) was obtained from local sources and used in the experimental procedures.

2.2. Synthesis of $\text{TiO}_2\text{-SiO}_2\text{-Fe}_2\text{O}_3$ NPs

In order to fix the adequate ratio between $\text{TiO}_2\text{-SiO}_2$ and Fe_2O_3 , different percentages were used and designated TS-1F, TS-2F, TS-3F, TS-5F, TS-10F, the compositions being $(40)\text{SiO}_2\text{-(}60 - x)\text{TiO}_2\text{-(}x)\text{Fe}_2\text{O}_3$, with x (wt%) = 1, 2, 3, 5, and 10%, respectively. They were combined and ground for two hours in a ceramic mortar before being calcined for four to six hours at $600 \text{ }^\circ\text{C}$. In order to choose the best material, we used an Evolution 220 UV–vis spectrophotometer (Thermo Fisher Scientific, Illkirch-Graffenstaden, France) to carry out an optical examination to assess the gap energy of each material, calculate the photoexcitation wavelength range, and evaluate the photodegradation efficiency. Due to the results detailed below, the percentage of the Fe_2O_3 compound was set at 1% for the remainder of the work.

2.3. Characterization

The morphology and elemental composition at the surface of the synthesized materials were examined using scanning electron microscopy (FEI Quanta 200, SEM model, Hillsboro, OR, USA). The crystalline phases were investigated using X-ray diffraction (Empyrean Panalytical diffractometer model, Malvern Panalytical, Malvern, UK) at 40 kV using $\text{Cu K}\alpha$ radiation ($\lambda = 1.54178 \text{ \AA}$). Fourier transform infrared (FT-IR) spectra were obtained with a Jasco 4200 (Tokyo, Japan) spectrometer in the $4000\text{--}400 \text{ cm}^{-1}$ range to investigate the functional characteristics of the materials. The reflectance spectra were obtained using

an Evolution 220 UV–visible spectrophotometer model. The Kubelka–Munk method was used to acquire the absorption spectra. A Shimadzu 6000 spectrophotometer (Kyoto, Japan) was employed to acquire photoluminescence spectra by exciting the sample with 330 nm radiation.

In addition, the point of zero charge for pH_{zpc} (pH value at which there is no net charge on the catalyst surface) was determined according to the following procedure. A series of bottles containing 50 mL of 0.1 M NaCl solutions were prepared. The pH of the bottles was adjusted to values from 2 to 10 by adding a few drops of 0.1 M NaOH or 0.1 M HCl aqueous solutions. Thereafter, each container received 0.15 g of dried catalyst. The suspensions were mixed for 48 h at room temperature at 150 rpm. After filtering each solution, a fresh pH reading named pH_{final} was obtained with a pH meter. Plotting of the $\text{pH}_{\text{final}} = f(\text{pH}_{\text{initial}})$ curve was done. The pH at which the curve crossed the first bisector line was identified as the pH_{zpc} value [25].

2.4. Photocatalytic Experiments

The photocatalytic activity of the synthesized materials was examined in a closed reactor. The reactor containing 100 mL of solution and 0.5 g of TS-xF was placed on an orbital shaker (Stuart SSL1, Paris, France) in a batch cylindrical glass reactor, which prevented any form of external light from passing through. The solution was stirred for 60 min at 20 °C to realize adsorption–desorption equilibrium. Photocatalytic tests were carried out with a 27 W UVA lamp (wavelength = 254 nm, Philips, Suresnes, France) and a 250 W «visible lamp» (high-pressure mercury), and photolysis tests were conducted without a semiconductor. In all experiments, the distance between the dye aqueous solution and the source was maintained constant at 10 cm. The following work was carried out with a TS-1F and 0.1 g/100 mL of semiconductor in the presence of sunlight. The supernatant was collected every 15 min. After that, a centrifugation at 10,509 RCF for 10 min occurred to separate the semiconductor from the RhB dye. The concentration was determined using a UV–vis spectrophotometer (PhotoLab 6100, Xylem, Washington, DC, USA) at the maximum absorption wavelength of RhB (555 nm). The photodegradation elimination efficiency % of RhB was determined according to the following equation:

$$\text{Elimination efficiency \%} = [(C_0 - C)/C_0] \times 100 \quad (1)$$

where C_0 is the initial concentration of RhB (mg L^{-1}) and C is the residual concentration of RhB (mg L^{-1}) after photodegradation.

In addition, the dye removal kinetics were obtained using the pseudo-first order non-linear model equation:

$$-dC/dt = kC \quad (2)$$

$$C_t = C_0 \exp(-kt) \quad (3)$$

where C_t is the concentration of the RhB dye at the known time t , k is the rate constant of pseudo-first order dye removal, and C_0 is the concentration of RhB at $t = 0$ min.

Recycling tests were carried out under the following conditions: $\text{pH} = 8$, $C_0 = 10 \text{ mg L}^{-1}$, $T = 25 \text{ }^\circ\text{C}$, and 0.1 g/100 mL semiconductor dosage. The photocatalyst was washed and dried after each use.

In addition, experiments with the addition of H_2O_2 were carried out to evaluate the effect of oxidant addition on the degradation rate of RhB. On the other hand, experiments were conducted to examine the effect of different free radicals on the photodegradation process of RhB using various scavengers, including EDTA, isopropanol, and acrylamide, which were tested as scavengers for h^+ , $\bullet\text{OH}$, and $\text{O}_2^{\bullet-}$, respectively [26,27].

3. Results and Discussion

3.1. Material Characterization

3.1.1. X-Ray Powder Diffraction

The crystalline structures of TiO_2 - SiO_2 , Fe_2O_3 , and the ternary composite TiO_2 - SiO_2 - Fe_2O_3 were examined using X-ray diffractograms. The high crystallinity of the materials was revealed by a series of highly intense peaks in the diffraction spectrum (Figure 1). The TiO_2 and SiO_2 crystalline phases were identified as tetragonal anatase (JCPDS 01-073-1764) and hexagonal silicon oxide (01-085-0794), respectively. The rhombohedral hematite phase (JCPDS 00-013-0534) was clearly identified for Fe_2O_3 . The ternary heterojunctions showed the presence of peaks characteristic of the three constituent phases, while the absence of additional phases confirmed the purity and the successful formation of the heterojunction (see Figure 1).

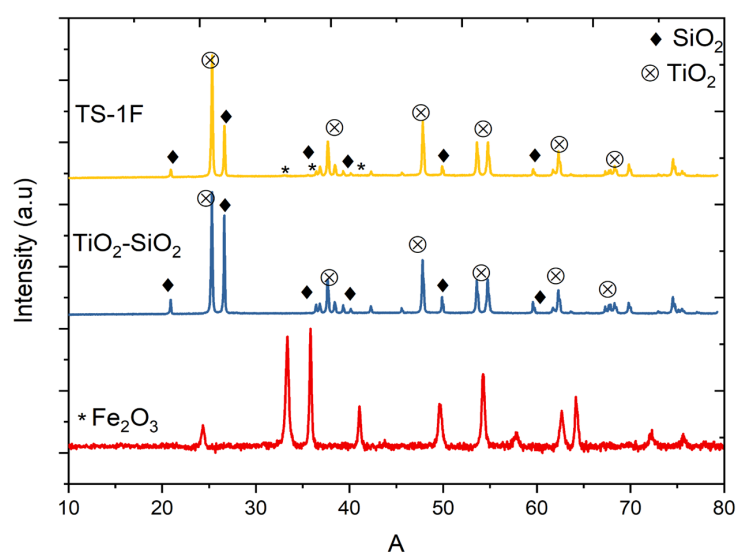


Figure 1. DRX spectra of Fe_2O_3 , TS, and TS-1F composite.

Average crystallite size was calculated by applying Scherrer's equation as:

$$D = 0.9\lambda / (\beta \cos \theta) \quad (4)$$

where D is the crystallite size (nm), β is the half-width of the diffraction band, θ is the Bragg diffraction angle (peak position in radians), and λ is the X-ray wavelength equal to 0.154 nm. Thus, the average crystallite size of the TS-1F was determined to be 36.05 nm [28,29].

3.1.2. Scanning Electron Microscopy-Energy Dispersive Spectroscopy (EDS-SEM)

Investigations were conducted using scanning electron microscopy (SEM) to examine the morphology of the nanomaterials. The morphologies of Fe_2O_3 (a), TiO_2 - SiO_2 (b), and the heterojunction TS-1F (c) are shown in Figure 2. It is evident that following the placement of Fe_2O_3 , the morphology of TS-1F underwent a significant change. Fe_2O_3 nanoparticles with a size of 22 nm were deposited homogeneously onto TiO_2 - SiO_2 nanoparticles (size = 35 nm). Furthermore, SiO_2 particles were larger than those of TiO_2 and Fe_2O_3 based on the data acquired, and TiO_2 - SiO_2 and Fe_2O_3 nanoparticles had strong contact with one another. The approximate size of the crystals determined from SEM data was within the 30–37 nm range, which was found to be comparable with X-ray diffraction observations. Furthermore, the elemental mapping spectra image shows the distribution of Fe_2O_3 on the surface of TiO_2 - SiO_2 at different ratios (1, 5, and 10%), as shown in Figure 3. The elements Ti, Si, and Fe were found to be uniformly distributed throughout the structures of the composites.

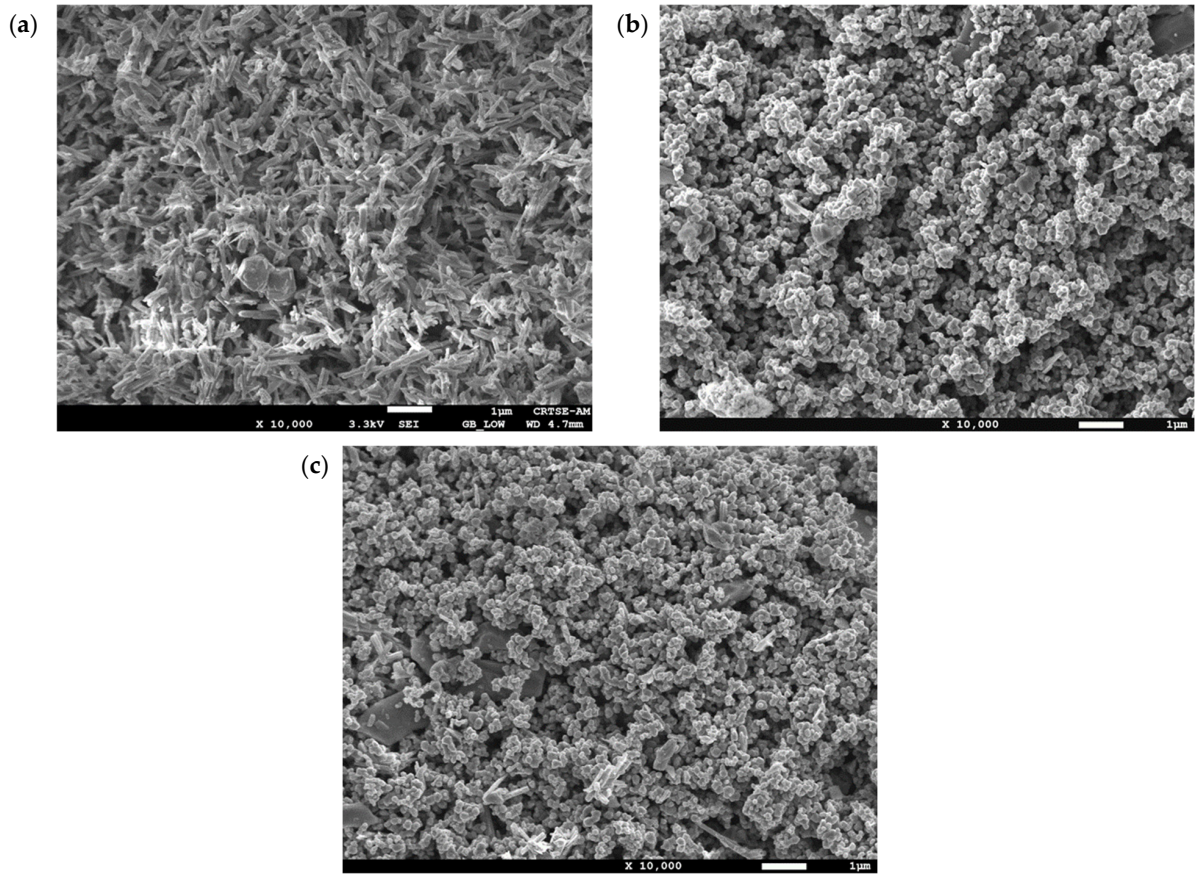


Figure 2. SEM images of (a) Fe_2O_3 , (b) $\text{TiO}_2\text{-SiO}_2$, (c) TS-1F.

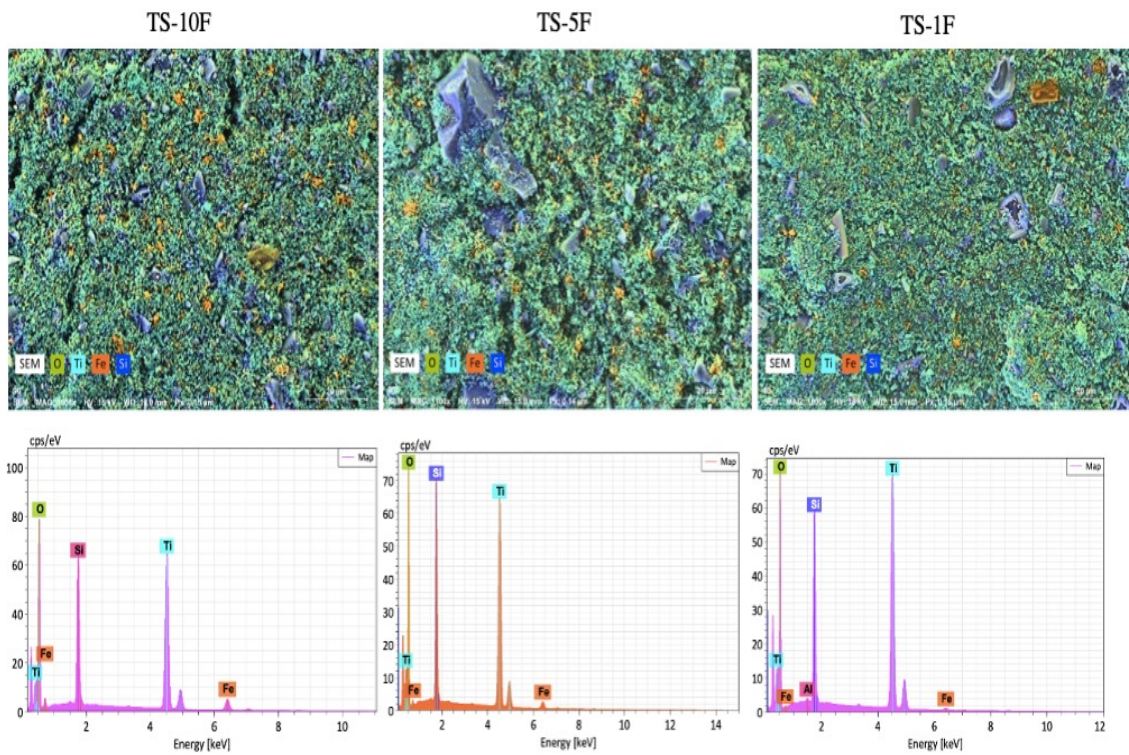


Figure 3. SEM-EDS mapping of TS-10F, TS-5F, and TF-1F.

3.1.3. Fourier Transform Infrared (FTIR) Spectroscopy

In this study, to investigate the optical characteristics of the synthesized material, the Fourier transform infrared (FTIR) spectra of the synthesized TiO_2 ; Fe_2O_3 ; and TS-1F, TS-3F, TS-5F, and TS-10F were recorded in the $4000\text{--}400\text{ cm}^{-1}$ range (Figure 4). For every graph, there were peaks seen at the following regions: 3670 cm^{-1} , $2970\text{--}3000\text{ cm}^{-1}$, 1403 cm^{-1} , 1250 cm^{-1} , and 800 cm^{-1} . The recorded peak at 800 cm^{-1} is indicative of Ti–O stretching. The peak at 1070 cm^{-1} is attributed to characteristic stretching vibration of Si–O–Si and Ti–O–Si bands in Ti- and Si-containing catalysts. Peaks between $1250\text{--}1800$ and 3000 cm^{-1} are typically linked to stretching of residual water molecules hydroxyl groups (OH). Additionally, peaks at 3600 cm^{-1} are indicative of the presence of $\text{TiO}_2/\text{Fe}_2\text{O}_3$ in the material.

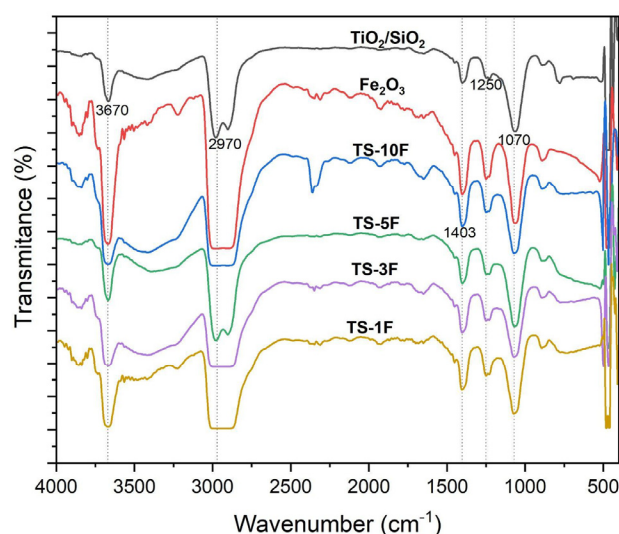


Figure 4. FTIR spectra of Fe_2O_3 ; $\text{TiO}_2\text{-SiO}_2$; and TS-1F, TS-3F, TS-5F, and TS-10F.

3.1.4. Optical Properties

The gap energy of the prepared materials was determined using the Kubelka–Munk equation:

$$(\alpha h\nu)^n = A(h\nu - E_g) \quad (5)$$

where α (cm^{-1}), ν (Hz), E_g (eV), h , and A are the absorption coefficient, light frequency, band gap energy, Planck's constant, and the Kubelka–Munk constant, respectively. In the case of a direct transition of the electron from the valence band to the conduction band, $n = 2$, whereas $n = 1/2$ in the case of an indirect transition [28]. On the basis of absorption spectra (Figure 5), plotting $(\alpha h\nu)^{1/2}$ versus $h\nu$ and extrapolating the absorption edge on the energy axis can give the forbidden energy. The intersection of the extrapolated tangent of the curve with the horizontal axis of this Tauc diagram gives the energies of the optical band gaps. The energies of the optical band gaps were 3.00, 1.39, and 2.87 eV for TiO_2 , Fe_2O_3 , and TS-1F, respectively. As a result, the bandgap energy of TS-1F (E_g) was lower than the bandgap energy of TiO_2 , which was attributed to the formation of a heterojunction structure between Fe_2O_3 , SiO_2 , and TiO_2 that enhanced the surface electric charge and allowed for easier transmission of photo-excited electrons. Figure 5a shows the UV–vis absorption spectra of the synthesized materials. The flat and large maximum at around 380 nm was attributed to the conversion of the TiO_2 energy gap and around 550 nm was attributed to Fe_2O_3 . For the binary heterojunction, all absorption curves indicated a redshift, and the band edge shifted to 430 nm. In addition, the prepared semiconductors had improved absorption of both UV and visible light. Photoactivity under visible light can be explained as follows: (i) Fe_2O_3 acts as a semiconductor and photosensitizer for TiO_2 , transporting photoexcited carriers to

TiO₂, and (ii) Fe³⁺ cations can form new miGAPs in the TiO₂ crystal lattice, allowing TiO₂ to be excited by visible light [29]. As mentioned by Abbas et al. (2016) [21], as a result, Fe has the potential to build up new energy levels in the bandgap of TiO₂ and reduce the gap between the valence and conduction band.

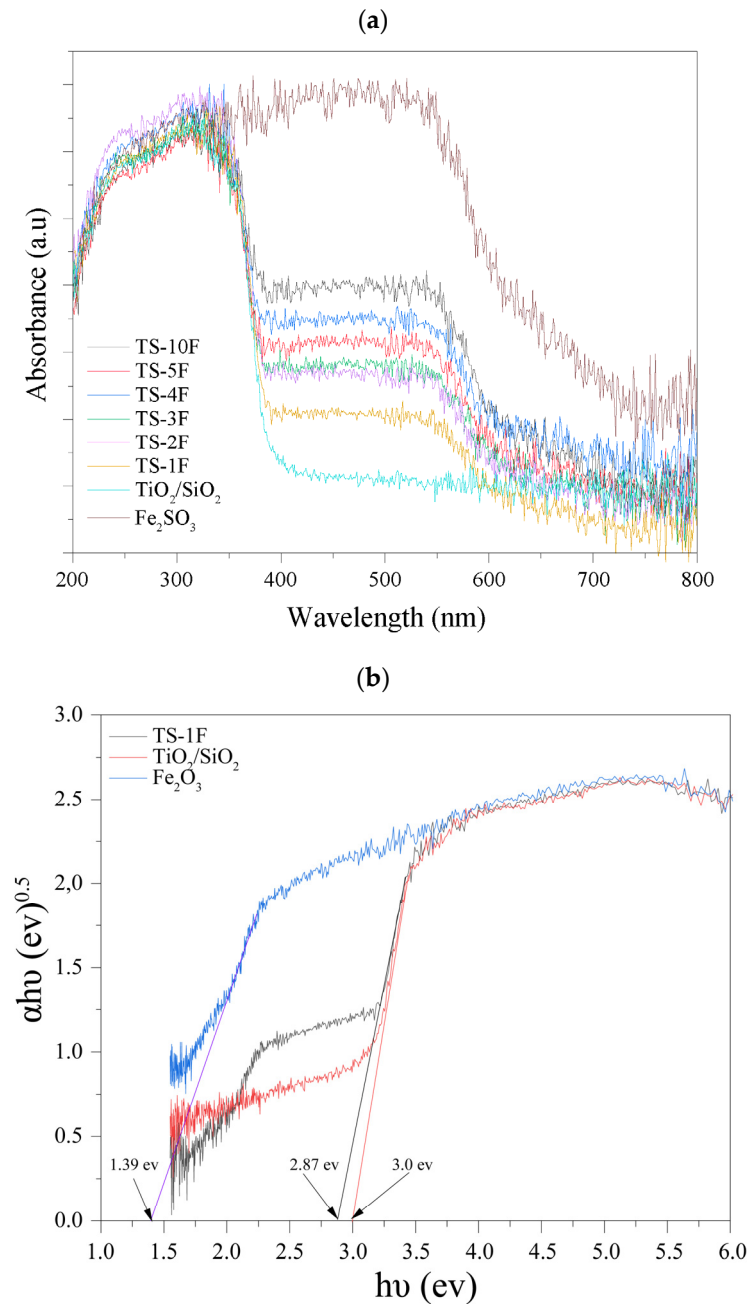


Figure 5. (a) UV-visible diffuse absorption spectra and (b) plots of $(\alpha h\nu)^{1/2}$ versus $h\nu$ for determination of gap energies.

3.1.5. Photoluminescence Spectra of the Prepared Samples

Photoluminescence (PL) spectroscopy was used (Figure 6) to investigate the efficiency of charge carrier recombination and separation in the photocatalysts. A high PL intensity signifies rapid recombination of photo-generated electrons and holes. Pure TiO₂ exhibited a strong PL signal, suggesting a high (e^-/h^+) recombination rate. In contrast, the hetero-junction photocatalyst TS-xF displayed a weaker PL intensity compared to pure TiO₂. This indicates a significant reduction in electron-hole recombination due to the formation of heterojunctions. Lower PL intensity typically translates to a lower recombination rate and,

consequently, enhanced photocatalytic activity. Among the synthesized catalysts, TS-1F (containing 1% Fe_2O_3) displayed the lowest PL intensity. This suggests that the 1% Fe_2O_3 addition most effectively inhibited the charge carriers and improved their lifetime.

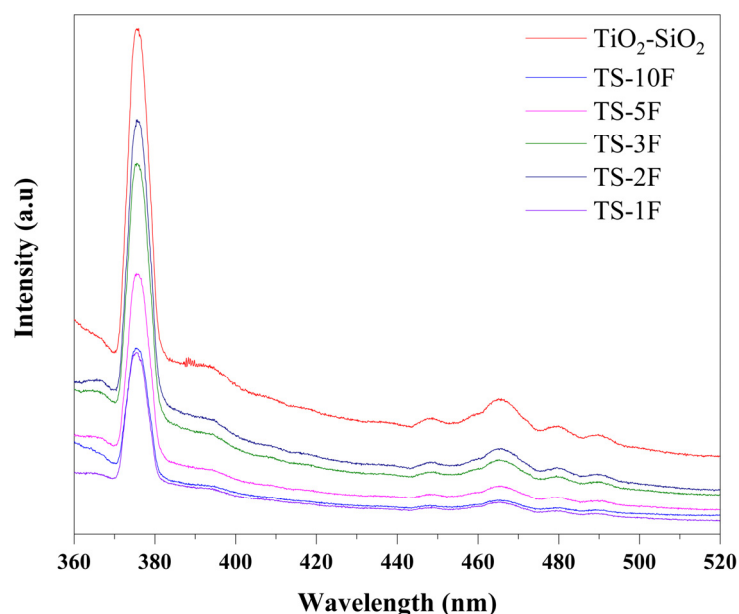


Figure 6. Photoluminescence spectra of different composites.

3.2. Photocatalysis Tests

The photocatalytic activity of the solids is dependent on a number of factors, including surface characteristics and light absorption capabilities as well as the rates of electron–hole reduction/oxidation. Basically, the effectiveness of photocatalysis can be decreased by a higher electron–hole recombination rate. In this sense, the photocatalytic activity will increase with the increasing specific surface area. The more surface area, the more defects there are, and the faster the recombination because the presence of faulty sites on the surface will cause increased recombination of the excited electrons and holes [19].

3.2.1. Under Visible Light (250 W) and Sunlight

The photocatalysis properties for the $\text{TiO}_2\text{-SiO}_2\text{-Fe}_2\text{O}_3$ heterojunction were investigated under visible light (250 W) and sunlight for the degradation of RhB dye. When the semiconductor is illuminated by photons with an energy higher than the band gap energy (E_g), a large number of electrons are promoted from the valence band (VB) to the conduction band (CB) of Fe_2O_3 , and holes are generated in the valence band [30]. Thus, it is believed that the mechanism of charge transport between the valence bands of Fe_2O_3 , SiO_2 , and TiO_2 effectively enhances the photocatalytic activity of the $\text{TiO}_2\text{-SiO}_2\text{-Fe}_2\text{O}_3$. It was documented that the presence of Fe cations can act as a mediator for the interfacial charge transfer, thus improving the life time of e^- and h^+ due to the electron–hole trapping at the Fe centers [31]. The heterojunction of Fe_2O_3 , SiO_2 , and TiO_2 not only facilitates the movement of electrons towards the conduction band but, due to the lower position of the conduction band, also acts as an electron–hole trap and reduces the electron–hole recombination time [32]. Decreasing the percentage of $\text{TiO}_2\text{-Fe}_2\text{O}_3$ negatively affected the degradation rate of RhB. This can be explained, according to the author, by increasing the recombination rate of charge carriers, which leads to competition with the redox reactions occurring on the surface of the photocatalyst. In another study [21], $\text{TiO}_2\text{-SiO}_2\text{-Fe}_2\text{O}_3$ nanoparticles synthesized with 1% of Fe_2O_3 showed the highest photocatalytic activity for RhB degradation.

The effect of the initial reactant concentration is a key factor in the photocatalytic degradation of pollutants. In general, the photocatalytic activity of TS-1F decreases with the increase in RhB concentration, which is probably due to the limited number of active sites available on the surface of the catalyst, as shown in Figures 7 and 8. Furthermore, TS1-F photocatalysis in the presence of sunlight was more significant than with visible light (250 W), which is intriguing from an economic standpoint because no energy was needed for the degradation. For 5, 10, and 15 ppm of RhB, 90% of degradation was attained only after 60 min in sunlight. In contrast, visible light degradation reached 60–80% after 135 min using the same concentrations. These outcomes demonstrate how successful TS1-F is as a photocatalyst. Table 1 represents the descriptive statistics of C/C_0 and inhibition percentage of RhB degradation under visible light (250 W) and sunlight.

Table 1. Descriptive statistics of C/C_0 and inhibition (%) for RhB degradation under either visible light or sunlight.

Type	Category	NB Time	Min	Max	Mean	Median	SD	CV
C/C_0								
Sunlight	5 ppm	14	0.063	0.218	0.077	0.064	0.011	52.913
	10 ppm	14	0.073	0.431	0.124	0.087	0.026	78.969
	15 ppm	14	0.041	0.703	0.126	0.078	0.047	138.134
	20 ppm	14	0.108	0.518	0.201	0.145	0.030	55.522
	25 ppm	14	0.106	0.644	0.363	0.394	0.049	50.324
	30 ppm	14	0.109	0.882	0.394	0.302	0.065	61.276
Visible light	5 ppm	10	0.215	0.988	0.523	0.460	0.079	47.843
	10 ppm	9	0.175	0.757	0.396	0.360	0.070	52.636
	15 ppm	11	0.273	0.836	0.490	0.455	0.048	32.726
	20 ppm	8	0.261	0.879	0.552	0.548	0.072	36.621
	25 ppm	13	0.113	0.809	0.478	0.461	0.060	45.062
	30 ppm	12	0.383	0.935	0.646	0.645	0.052	27.993
% Inhibition								
Sunlight	5 ppm	14	78.182	93.709	92.288	93.636	1.091	4.422
	10 ppm	14	56.881	92.661	87.615	91.284	2.614	11.163
	15 ppm	14	29.730	95.946	87.404	92.230	4.650	19.908
	20 ppm	14	48.193	89.157	79.865	85.542	2.988	13.998
	25 ppm	14	35.577	89.454	63.670	60.577	4.886	28.715
	30 ppm	14	11.777	89.096	60.634	69.759	6.447	39.782
Visible light	5 ppm	10	1.181	78.543	47.658	54.035	7.919	52.547
	10 ppm	9	24.318	82.463	60.414	63.991	6.946	34.490
	15 ppm	11	16.361	72.732	51.004	54.536	4.835	31.438
	20 ppm	8	12.152	73.928	44.780	45.203	7.150	45.159
	25 ppm	13	19.139	88.715	52.249	53.927	5.968	41.183
	30 ppm	12	6.533	61.708	35.441	35.527	5.217	50.992

Notes: NB: Number of times. In this study, we proposed 14 times points: 15, 30, 45, 60, 75, 90, 105, 120, 135, 150, 165, 180, 195, and 210 min. Min: minimum; Max: maximum; SD: standard deviation; CV: coefficient of variation (%).

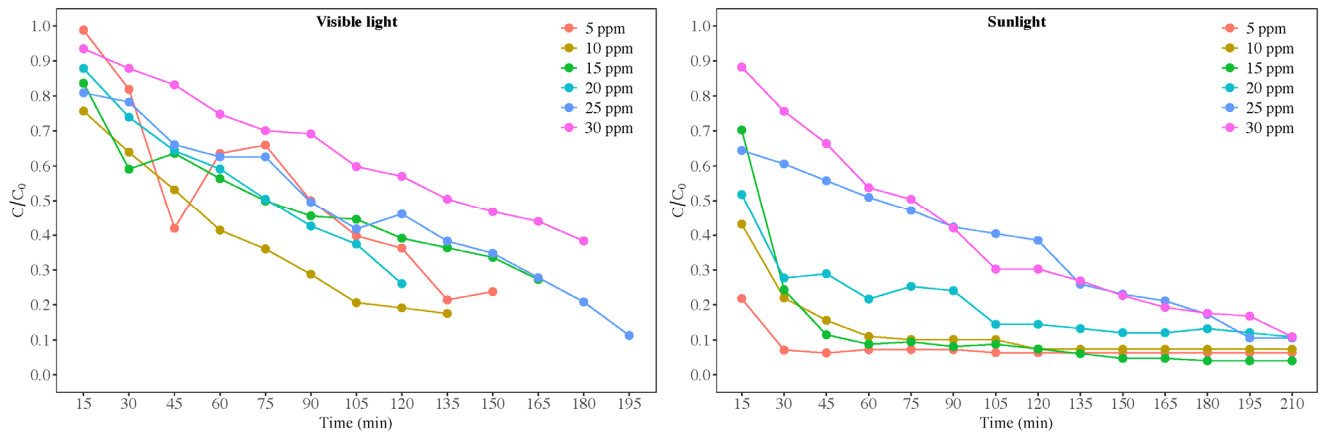


Figure 7. The effect of RhB concentration on the photocatalytic activity of the TS-1F heterojunction under visible light (250 W) (left) and sunlight (right).

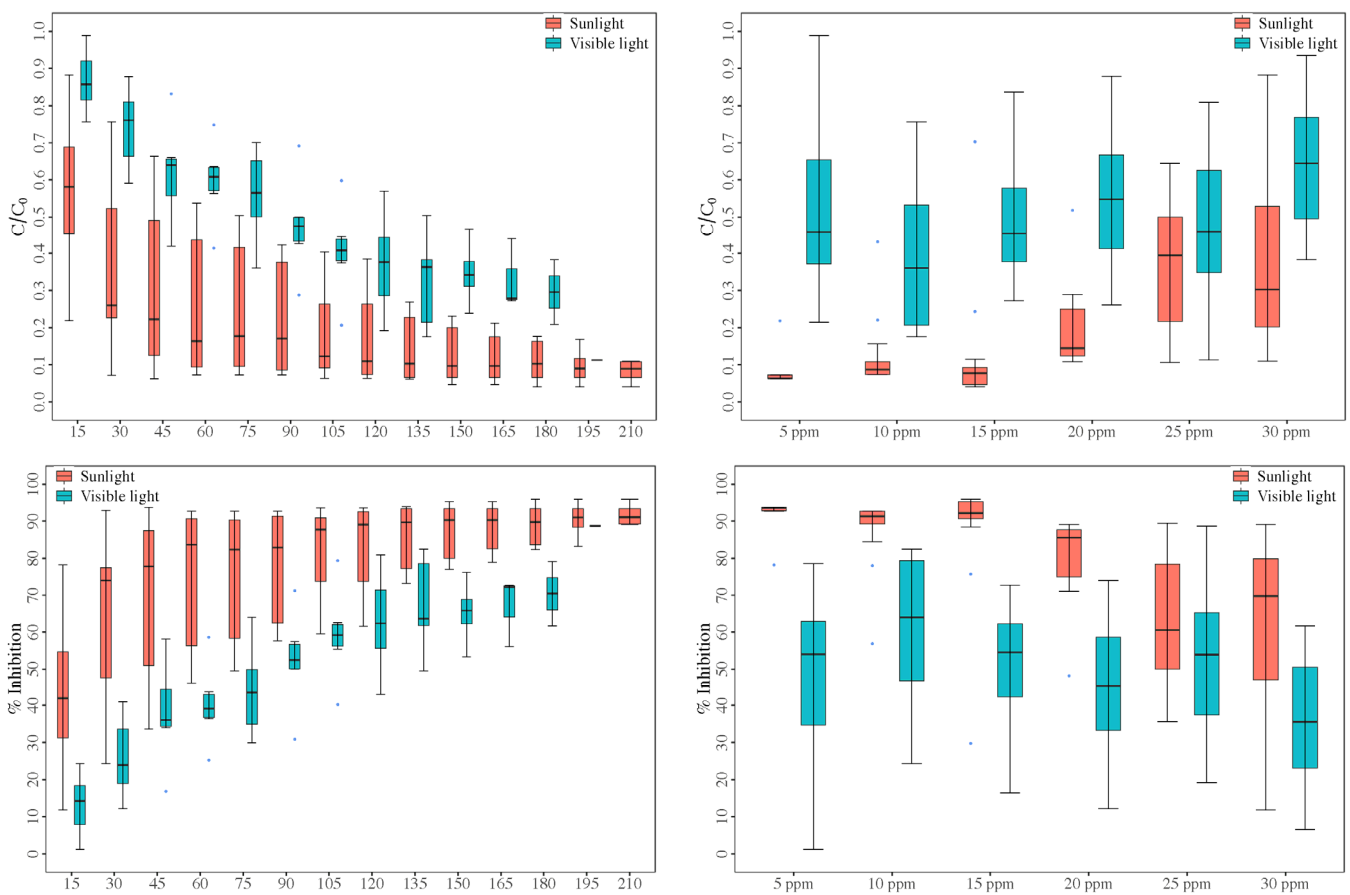
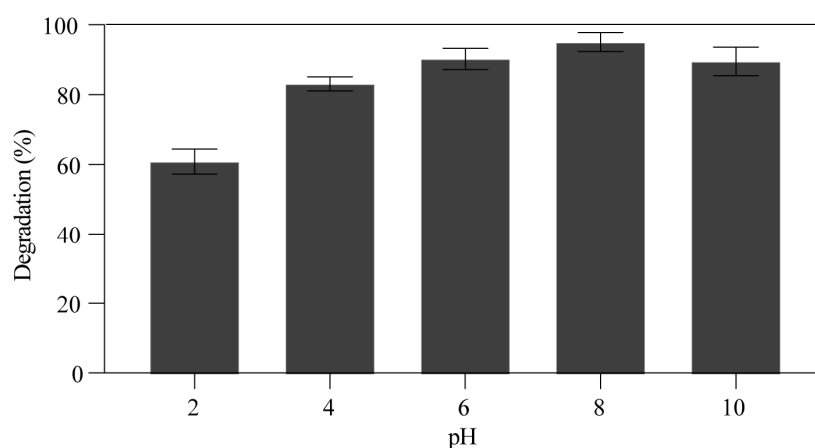


Figure 8. Boxplots of C/C_0 and % inhibition for both sunlight and visible light.

To further explore this photocatalyst regarding the elimination of RhB dye under several conditions, pH levels following 210 min of sun exposure were varied, as shown in Table 2; Figure 9 shows the resulting degradation rate as a function of pH.

Table 2. Effect of pH on the degradation rate constant (k) of RhB using the TS-1F photocatalyst under sunlight.

pH Value	k (10^{-4} min^{-1})	R Squared COD	Adj. R-Squared
2	37.7 ± 2.76	0.94	0.93
6	96.7 ± 6.11	0.96	0.96
8	100 ± 2.41	0.99	0.99
10	143.7 ± 5.45	0.99	0.98

**Figure 9.** Effect of pH values on the degradation rate under sunlight, $C_0 = 10$ ppm, TS-1F = 1 g/L, and 210 min.

The concentration of the dye fell as the illumination period increased, as predicted, and after each 15 min time interval, the percentage of dye degradation was observed. It was consistent with the first-order kinetic behavior proposed by the Langmuir–Hinshelwood model. As can be observed, the greatest efficiency of RhB degradation was obtained at an acidic pH of 10. pH is crucial to the destruction of pollutants in the photocatalytic process, and this may be because of variations in the photocatalyst surface charge. The pH of the solution influences the electrostatic interactions that occur between solvent molecules, charged radicals produced during photocatalytic oxidation, and the semi-conductive surface. Indeed, TS-1F may aggregate at $\text{pH} = 2$ due to a high concentration of H^+ , which reduce the contact surface area. At a $\text{pH} < 3.22$ ($\text{pK}_a = 3.22$), according to Mchedlov-Petrosyan et al., the carboxyl group of RhB remains in a RhB^+ cationic form, which produces an electrostatic repulsion between the positively charged TS-1F and RhB [33]. On the other hand, at pH 6 (lower than $\text{pH}_{\text{zpc}} = 8$), it gives the catalyst surface a net positive charge, which favors anion adsorption and reduces the interaction of the cationic pollutant RhB with catalyst sites. When the pH of the solution is higher than pH_{zpc} , and as the pH increases, the net surface charge becomes more negative, favoring the adsorption of cations by electrostatic attraction, as occurs at pH 8 and pH 10.

3.2.2. The Synergetic Effect of H_2O_2 -Assisted Photocatalytic Degradation

The sunlight absorption of RhB with different amounts of H_2O_2 (20 μL , 50 μL , 100 μL , and 200 μL) and in the presence of TS-1F at a fixed reaction time was investigated. H_2O_2 is an electron acceptor that is more potent than oxygen due to its high oxidation potential and electrophilic nature. Several studies using deoxygenated semiconductor solutions were carried out to assess how the dosage of H_2O_2 affected the photocatalytic degradation of the dye contaminants [34–36]. The first-order degradation rate constant (k) of RhB was sensitive to the addition of H_2O_2 with values of $(115.3 \pm 3.5) \times 10^{-4} \text{ min}^{-1}$ and $(87.1 \pm 5.2) \times 10^{-4} \text{ min}^{-1}$ with and without H_2O_2 addition, respectively.

Therefore, it was anticipated that adding H_2O_2 to the photocatalytic system would accelerate RhB degradation. However, a high amount of H_2O_2 ($>50 \mu\text{L}$ H_2O_2) might decrease the degradation rate, which can be attributed to the competitive adsorption of the oxidant on the catalyst surface and the production of complexes, including $\text{Ti}(\text{O}_2)(\text{OH})_2$ and $\text{Ti}(\text{OOH})(\text{OH})_3$. In addition, it reacts with the hydroxyl radical, thus acting as a scavenger [37]. The addition of H_2O_2 traps electrons in the photocatalyst conduction band, preventing them from recombining with the conduction band. This mechanism offers a number of advantages, including reduced recombination time, enabling electrons to participate in degradation reactions.

According to Figure 10, the higher reaction rates after the addition of peroxide were attributed to the increase in the concentration of the hydroxyl radical. According to our findings, when adding a low amount of H_2O_2 ($50 \mu\text{L}$), the degradation rate increased to 88.6%. According to a previous study, a low concentration of H_2O_2 inhibited the electron-hole recombination and could act as an alternative electron acceptor to oxygen since H_2O_2 is a better electron acceptor than molecular oxygen [37]. However, after the addition of $100 \mu\text{L}$ of H_2O_2 , the degradation rate decreased to 81.2% and to 78.4% for $200 \mu\text{L}$. This could be due to the scavenging effect as $\bullet\text{OH}$ became predominant [38]. The amount of $\bullet\text{OH}$ radicals produced and the amount of $\bullet\text{OH}$ radicals captured can be used to describe how H_2O_2 addition affects RhB breakdown.

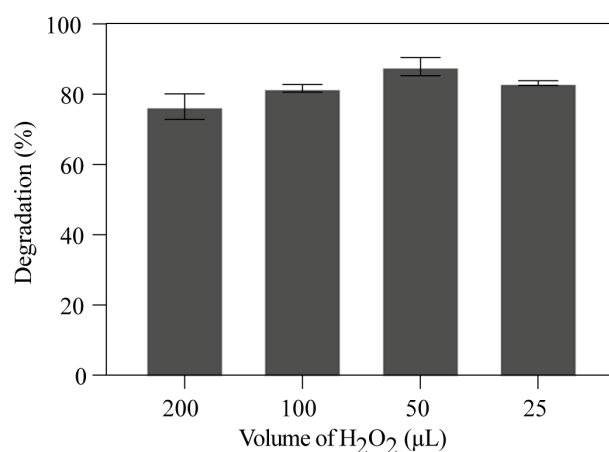


Figure 10. Effect of H_2O_2 on RhB removal under sunlight, pH 8, $C_0 = 10$ ppm, TS-1F = 1 g/L, and 210 min.

3.2.3. The Effect of TS-1F Dosage on the Degradation Rate of RhB

This study investigated the effect of catalyst dosage on the photodegradation of RhB under sunlight in the range from 0.1 to 0.6 g/100 mL. As a result, increasing the loading of the catalyst up to 0.4 g/100 mL slightly decreased the removal rate of RhB from 96% to 93%. This can be attributed to the turbidity of the solution, which can play an obstacle to the penetration of solar radiation, as shown in Figure 11. This could be explained by the turbidity resulting in the mixture, which somehow blocked the penetration of light into the solution and thereafter blocked the generation of free radicals.

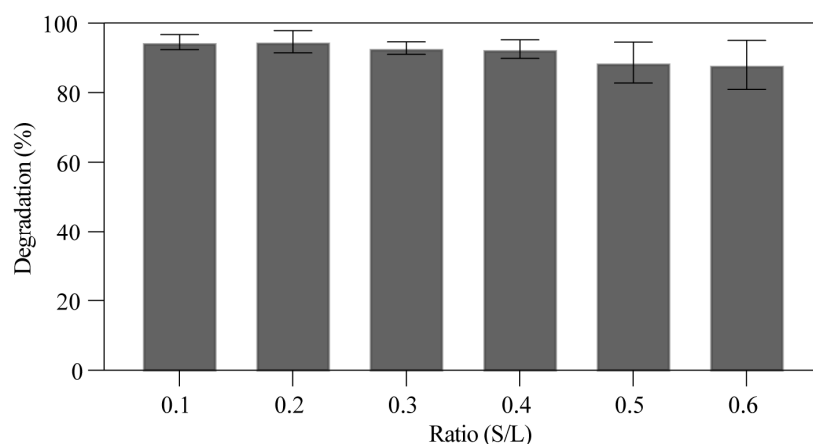


Figure 11. Effect of TS-1F ratio on the degradation efficiency under sunlight, pH 8, $C_0 = 10$ ppm, and 210 min.

3.2.4. An Assessment of $\text{TiO}_2\text{-SiO}_2\text{-Fe}_2\text{O}_3$ Heterojunction Reusability and Recyclability

The regeneration of TS-1F is essential in order to get an idea of its stability during repetitive cycles [39]. The reuse of TS-1F (0.1 g/100 mL and pH 8) was studied. According to Figure 12, the TS-1F photocatalyst can be reusable through three consecutive cycles of combined adsorption-photodegradation removal of RhB. It was found that RhB removal was recorded in all cycles with and without washing. In the first and the second cycles, the degradation rates surpassed 90% for RhB removal for more than 3 h (210 min) of photocatalysis under sunlight. However, the degradation rate was affected in the third cycle (63.4%) for the semi-conductor without washing. The decrease in the degradation efficiency might have resulted from the accumulation of the degradation product on the surface of the photocatalyst, thereby blocking the active sites, since the photocatalyst was not separated and washed after each cycle to minimize the number of steps and water consumption. Therefore, it could be repeatedly used as desired (with washing) in practical applications, which could improve economic efficiency, ensuring its applicability for real-world applications by reducing the material cost.

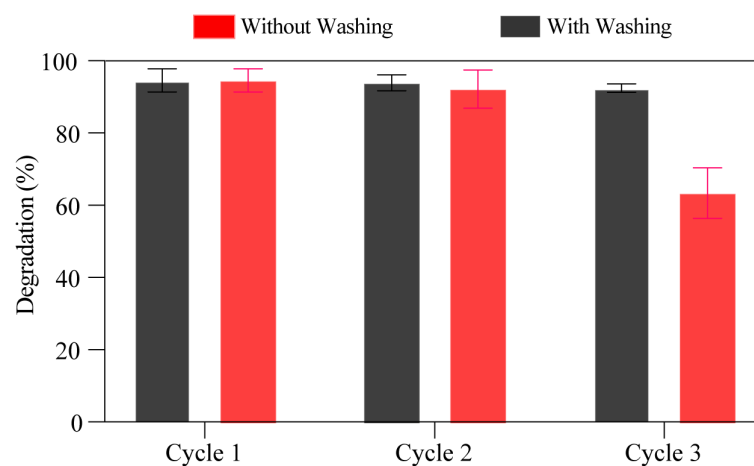


Figure 12. Recovery performance and stability of TS-1F degradation of RhB under sunlight, pH 8, $C_0 = 10$ ppm, TS-1F = 1 g/L, and 210 min.

3.3. Scavenger Effect

The active species that are crucial in semiconductor photocatalysis are still the subject of much debate due to their complexity. Free radical capture experiments were carried out with the addition of 5 mM radical scavengers, namely ethylenediamine tetraacetic acid

(EDTA), methanol (MeOH), and acrylamide (AM), which are added as trapping agents for h^+ , hydroxyl radicals ($\bullet OH$), and superoxide radicals ($O_2^{\bullet -}$), at pH 8, an initial catalyst concentration of 0.1 g/100 mL, and 10 ppm of RhB. This was done to investigate the primary active species and catalytic mechanism of $TiO_2-SiO_2-Fe_2O_3$ photocatalytic degradation of RhB. Alcohols like methanol are frequently used as scavengers of hydroxyl radicals [40]; nevertheless, after 2.5 h, the percentage of RhB degradation only reached 60%, indicating the importance of hydroxyl radicals in the breakdown of RhB. Alcohols like methanol can compete with substrates for TiO_2 reaction sites, although their main function is to scavenge free $\bullet OH$ radicals. Nevertheless, a number of studies have shown the usage of these alcohols as hole scavengers [41,42]. Furthermore, to investigate the elimination of RhB using photocatalysis, EDTA was utilized as a hole scavenging agent. The following could be the response between the H^+ species and the organic hole scavenger.



Acrylamide was used in this study as singlet oxygen scavenger; as shown in Figure 13, the degradation rate of RhB decreased significantly after its addition, even at 5 mM. This proves that singlet oxygen is an important species for the catalytic process since the latter will be generated under light exposure. The generation of singlet oxygen is usually the proposed mechanism responsible for pollutant breakdown and its removal from the aqueous medium. The synthetic TS-1F responds to the aforementioned circumstances, which makes it a promising material for water purification.

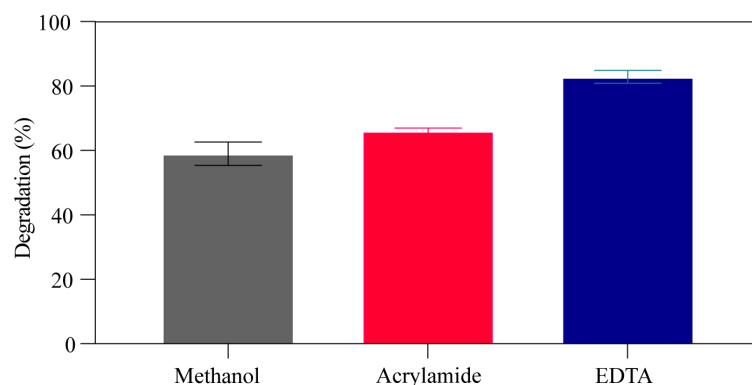
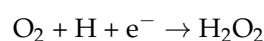
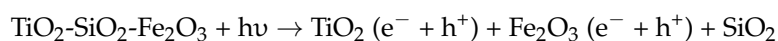


Figure 13. Effect of scavenger on photodegradation of RB, where TS-1F under sunlight $C_0 = 10$ mg/L, TS-1F = 0.1 g/100 mL, pH = 8, and $C_{\text{scavenger}} = 5$ mM after 150 min.

3.4. Degradation Mechanism

The gap energy of Fe_2O_3 is lower than that of TiO_2 ; after excitation with sunlight, electrons migrate from Fe_2O_3 to TiO_2 and holes from TiO_2 to Fe_2O_3 under the influence of sunlight [43]. Due to the migration of charge carriers, electrons accumulate mainly in the conduction band of TiO_2 and reduce dissolved oxygen to generate superoxide radicals $\bullet O_2$. The electrons in the TiO_2 valence band (VB) transfer easily to the CB under the effect of electrostatic force. However, the conduction band (CB) potential of TiO_2 (-0.6 eV) is more negative than the $O_2/O_2^{\bullet -}$ potential $E_0(O_2/O_2^{\bullet -}) = -0.33$ eV. The electrons are therefore unable to reduce oxygen molecules in the atmosphere to generate $O_2^{\bullet -}$; on the other hand, if the electrons are more negative than $E_0(O_2/H_2O_2) = 0.682$ eV, then the TiO_2 electrons can reduce the captured oxygen to H_2O_2 (Figure 14).



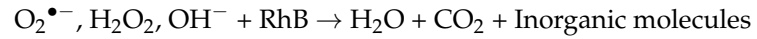
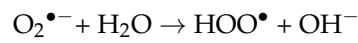
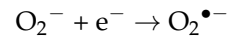
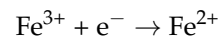
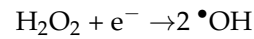


Figure 14. The suggested mechanism of RhB degradation using TS-1F under sunlight.

3.5. Cost Analysis

The cost analysis considered the entire cost of RhB degradation as well as the cost of each grade of chemical utilized to produce the composite as well as to degrade 30 ppm of RhB dye. As a result, the cost of the chemicals used in this study was 0.75 € per experiment, and the energy used by the equipment was limited to 1.95 €. The quantity, cost, and price of each chemical are summarized in Table 3. Based on the collected data, the cost analysis showed that the overall expense was about 2.7 € for each experiment. The current study was carried out in the presence of sun radiation, which lowered the treatment's operational costs. Previous studies used external energy, such as visible or ultraviolet light, for treatment and resulted in increased operational expenses [44,45].

Table 3. Cost analysis for the preparation of 0.1 g heterojunction $\text{TiO}_2\text{-SiO}_2\text{-Fe}_2\text{O}_3$ for RhB degradation.

Chemicals Used	Amount per Experiment	Cost (€)	Total Cost (€)
TiO ₂ /SiO ₂	0.05 g	0.65	0.75
Fe ₂ O ₃	0.05 g	0.10	
HCl/NaOH	Drops	-	
H ₂ O ₂	25–200 µL	0.01	
Equipment	Energy Consumed	Cost (€)	Total Cost (€)
Calcination oven (1200 W)	6 h (for the whole study)	1.16	1.95
Magnetic stirrer (610 W)	3 h	0.29	
Refrigerated centrifuge (720 W)	30 min in total	0.11	
Water purificator	3 L	0.39	

4. Conclusions

In order to achieve industrial photocatalytic degradation of organic pollutants beyond conventional treatment procedures, as well as finding a successful replacement for traditional treatment methods that need a lot of energy, it is noteworthy to prepare visible light-active photocatalysts by improving the operating parameters. When it comes to the photodegradation of RhB dye at 30 ppm under sunlight, TS-1F synthesized in this work showed increased catalytic activity (>90%), which was more interesting than that under visible light (>70%).

In this study, solid UV–visible spectroscopy with FTIR spectroscopy confirmed the formation of TiO₂-SiO₂-Fe₂O₃ nanocomposites as well as the reduced gap energy (2.87 eV). The SEM-EDS mapping revealed the morphology and the proportions of the elements present in these composites. The photocatalytic activity of 59TiO₂-40SiO₂-1Fe₂O₃ (TS-1F) semiconductors has excellent photostability and recyclability properties, making them ideal for practical applications.

The photocatalytic mechanism of degradation was predicted on the basis of scavenging experiments which revealed that O₂^{•−} and [•]OH radicals are reactive species. From an economic standpoint, the resulting material was interesting in terms of cost and reusability. Due to their appealing qualities and benefits, these sensitized photocatalysts are highly sought-after candidates in the field of photocatalysis.

Author Contributions: S.O.T. and L.M.: investigation, original draft writing, formal analysis, methodology; A.A., L.M. and L.B.: project administration, validation, supervision; R.B., S.O.T. and L.M.: writing, methodology; J.-C.B., L.M. and S.S.: supervision, validation, reviewing, editing; L.M., M.N.A., A.A. and S.S.: reviewing, editing; M.I.K. and M.N.A.: data curation, methodology; A.T. and M.N.A.: software, data curation; L.B., A.T., R.B. and M.N.A.: funding, resources; L.M. and S.O.T.: conceptualization, writing, validation, project administration, supervision. All authors have read and agreed to the published version of the manuscript.

Funding: This work was funded by (PNURSP2025R481), Princess Nourah bint Abdulrahman University, Riyadh, Saudi Arabia.

Data Availability Statement: Data available on request.

Acknowledgments: The authors are grateful to Princess Nourah bint Abdulrahman University Researchers Supporting Project number (PNURSP2025R481), Princess Nourah bint Abdulrahman University, Riyadh, Saudi Arabia.

Conflicts of Interest: The authors declare that they have no known competing financial interests or personal relationships that could have appeared to influence the work reported in this paper.

References

1. Prakash, O.; Maurya, S.; Tripathy, P.; Sharma, A.; Vijay, R.; Pal, S. Chapter 21—Nano- and phytoremediation technique for textile wastewater treatment and successive production of fertilizers. In *Metagenomics to Bioremediation*; Kumar, V., Bilal, M., Shahi, S.K., Garg, V.K., Eds.; Developments in Applied Microbiology and Biotechnology; Academic Press: Cambridge, MA, USA, 2023; pp. 537–559. ISBN 978-0-323-96113-4. [[CrossRef](#)]
2. Berradi, M.; Hsissou, R.; Khudhair, M.; Assouag, M.; Cherkaoui, O.; Bachiri, A.E.; Harfi, A.E. Textile finishing dyes and their impact on aquatic environs. *Heliyon* **2019**, *5*, e02711. [[CrossRef](#)]
3. Elsayed, M.; Abdel-Raouf, M.E.-S. Wastewater Treatment Methodologies, Review Article. *Int. J. Environ. Agric. Sci.* **2019**, *3*, 18.
4. Boudraa, R.; Talantikite-Touati, D.; Souici, A.; Djermoune, A.; Saidani, A.; Fendi, K.; Amrane, A.; Bollinger, J.-C.; Nguyen Tran, H.; Hadadi, A.; et al. Optical and photocatalytic properties of TiO₂-Bi₂O₃-CuO supported on natural zeolite for removing Safranin-O dye from water and wastewater. *J. Photochem. Photobiol. A Chem.* **2023**, *443*, 114845. [[CrossRef](#)]
5. Mouni, L.; Belkhiri, L.; Bollinger, J.-C.; Bouzaza, A.; Assadi, A.; Tirri, A.; Dahmoune, F.; Madani, K.; Remini, H. Removal of Methylene Blue from aqueous solutions by adsorption on Kaolin: Kinetic and equilibrium studies. *Appl. Clay Sci.* **2018**, *153*, 38–45. [[CrossRef](#)]

6. Imessaoudene, A.; Cheikh, S.; Hadadi, A.; Hamri, N.; Bollinger, J.-C.; Amrane, A.; Tahraoui, H.; Manseri, A.; Mouni, L. Adsorption Performance of Zeolite for the Removal of Congo Red Dye: Factorial Design Experiments, Kinetic, and Equilibrium Studies. *Separations* **2023**, *10*, 57. [[CrossRef](#)]
7. Merdoud, R.; Aoudjit, F.; Mouni, L.; Ranade, V.V. Degradation of methyl orange using hydrodynamic Cavitation, H₂O₂, and photo-catalysis with TiO₂-Coated glass Fibers: Key operating parameters and synergistic effects. *Ultrason. Sonochem.* **2024**, *103*, 106772. [[CrossRef](#)]
8. Hadadi, A.; Imessaoudene, A.; Bollinger, J.-C.; Cheikh, S.; Assadi, A.A.; Amrane, A.; Kebir, M.; Mouni, L. Parametrical Study for the Effective Removal of Mordant Black 11 from Synthetic Solutions: Moringa oleifera Seeds' Extracts Versus Alum. *Water* **2022**, *14*, 4109. [[CrossRef](#)]
9. Boudraa, R.; Talantikite-Touati, D.; Djermoune, A.; Souici, A.; Kebir, M.; Merzeg, F.A.; Amrane, A.; Bollinger, J.-C.; Mouni, L. Comprehensive Characterization and Unprecedented Photocatalytic Efficacy of TiO₂-CuO-La₂O₃ and TiO₂-CuO-Bi₂O₃ Nanocomposites: A Novel Approach to Environmental Remediation. *Mater. Sci. Eng. B* **2025**, *312*, 117863. [[CrossRef](#)]
10. Imessaoudene, A.; Mechraoui, O.; Aberkane, B.; Benabbas, A.; Manseri, A.; Moussaoui, Y.; Bollinger, J.-C.; Amrane, A.; Zoukel, A.; Mouni, L. Synthesis of a TiO₂/zeolite composite: Evaluation of adsorption-photodegradation synergy for the removal of Malachite Green, Nano-Struct. *Nano-Objects* **2024**, *38*, 101191. [[CrossRef](#)]
11. Hassaan, M.A.; El-Nemr, M.A.; Elkatory, M.R.; Ragab, S.; Niculescu, V.-C.; El Nemr, A. Principles of Photocatalysts and Their Different Applications: A Review. *Top. Curr. Chem.* **2023**, *381*, 31. [[CrossRef](#)] [[PubMed](#)]
12. Raj, K.J.A.; Smith, Y.R.; Subramanian, V.; Viswanathan, B. Structural studies of silica modified titania and its photocatalytic activity of 4-chlorophenol oxidation in aqueous medium. *Indian J. Chem.-Sect. A* **2010**, *49*, 867.
13. Babyszko, A.; Wanag, A.; Sadłowski, M.; Kusiak-Nejman, E.; Morawski, A.W. Synthesis and Characterization of SiO₂/TiO₂ as Photocatalyst on Methylene Blue Degradation. *Catalysts* **2022**, *12*, 1372. [[CrossRef](#)]
14. Ramamoorthy, V.; Kannan, K.; Joice Joseph, A.I.; Kanagaraj, T.; Thiripuranthagan, S. Photocatalytic degradation of acid orange dye using silver impregnated TiO₂/SiO₂ composite catalysts. *J. Nanosci. Nanotechnol.* **2016**, *16*, 9980–9986. [[CrossRef](#)]
15. Chun, H.; Yizhong, W.; Hongxiao, T. Influence of adsorption on the photodegradation of various dyes using surface bond-conjugated TiO₂/SiO₂ photocatalyst. *Appl. Catal. B Environ.* **2001**, *35*, 95–105. [[CrossRef](#)]
16. Xie, C.; Xu, Z.; Yang, Q.; Xue, B.; Du, Y.; Zhang, J. Enhanced photocatalytic activity of titania-silica mixed oxide prepared via basic hydrolyzation. *Mater. Sci. Eng. B* **2004**, *112*, 34–41. [[CrossRef](#)]
17. Ding, Z.; Lu, G.Q.; Greenfield, P.F. Role of the Crystallite Phase of TiO₂ in Heterogeneous Photocatalysis for Phenol Oxidation in Water. *J. Phys. Chem. B* **2000**, *104*, 4815–4820. [[CrossRef](#)]
18. Joseph, C.G.; Taufiq-Yap, Y.H.; Musta, B.; Sarjadi, M.S.; Elilarasi, L. Application of Plasmonic Metal Nanoparticles in TiO₂-SiO₂ Composite as an Efficient Solar-Activated Photocatalyst: A Review Paper. *Front. Chem.* **2021**, *8*, 568063. [[CrossRef](#)]
19. Fawzi Suleiman Khasawneh, O.; Palaniandy, P. Removal of organic pollutants from water by Fe₂O₃/TiO₂ based photocatalytic degradation: A review. *Environ. Technol. Innov.* **2021**, *21*, 101230. [[CrossRef](#)]
20. Johngika, J.; Harun, Z. Review On the Biosynthesis of Composite TiO₂—Inorganic/Metal Oxide (Fe₂O₃): Photocatalytic and Antibacterial Purpose Of Wastewater Treatment. *Res. Prog. Mech. Manuf. Eng.* **2023**, *4*, 504–517.
21. Abbas, N.; Shao, G.N.; Haider, M.S.; Imran, S.M.; Park, S.S.; Kim, H.T. Sol-gel synthesis of TiO₂-Fe₂O₃ systems: Effects of Fe₂O₃ content and their photocatalytic properties. *J. Ind. Eng. Chem.* **2016**, *39*, 112–120. [[CrossRef](#)]
22. Wu, L.; Yan, H.; Xiao, J.; Li, X.; Wang, X.; Zhao, T. Characterization and photocatalytic properties of nano-Fe₂O₃-TiO₂ composites prepared through the gaseous detonation method. *Ceram. Int.* **2017**, *43*, 14334–14339. [[CrossRef](#)]
23. Baniamerian, H.; Teimoori, M.; Saberi, M. Fe₂O₃/TiO₂/Activated Carbon Nanocomposite with Synergistic Effect of Adsorption and Photocatalysis. *Chem. Eng. Technol.* **2021**, *44*, 130–139. [[CrossRef](#)]
24. Zhou, W.; Fu, H.; Pan, K.; Tian, C.; Qu, Y.; Lu, P.; Sun, C.-C. Mesoporous TiO₂/α-Fe₂O₃: Bifunctional Composites for Effective Elimination of Arsenite Contamination through Simultaneous Photocatalytic Oxidation and Adsorption. *J. Phys. Chem. C* **2008**, *112*, 19584–19589. [[CrossRef](#)]
25. Fiol, N.; Villaescusa, I. Determination of sorbent point zero charge: Usefulness in sorption studies. *Environ. Chem. Lett.* **2009**, *7*, 79–84. [[CrossRef](#)]
26. Labaran, B.A.; Vohra, M.S. Photocatalytic removal of selenite and selenate species: Effect of EDTA and other process variables. *Environ. Technol.* **2014**, *35*, 1091–1100. [[CrossRef](#)]
27. Boudraa, R.; Talantikite-Touati, D.; Souici, A.; Djermoune, K.; Amrane, A.; Bollinger, J.-C.; Tran, H.N.; Mouni, L. Breaking new grounds: Solid-state synthesis of TiO₂-La₂O₃-CuO nanocomposites for degrading brilliant green dye under visible light. *J. Clean. Prod.* **2024**, *481*, 144126. [[CrossRef](#)]
28. Lee, W.-G.; Chae, S.; Chung, Y.K.; Yoon, W.-S.; Choi, J.-Y.; Huh, J. Indirect-To-Direct Band Gap Transition of One-Dimensional V₂Se₉: Theoretical Study with Dispersion Energy Correction. *ACS Omega* **2019**, *4*, 18392–18397. [[CrossRef](#)]

29. Kavitha, S.; Ranjith, R.; Jayamani, N.; Vignesh, S.; Palanivel, B.; Djellabi, R.; Bianchi, C.L.; Alharthi, F.A. Fabrication of visible-light-responsive TiO₂/α-Fe₂O₃-heterostructured composite for rapid photo-oxidation of organic pollutants in water. *J. Mater. Sci. Mater. Electron.* **2022**, *33*, 8906–8919. [[CrossRef](#)]
30. Zhang, R.; Sun, M.; Zhao, G.; Yin, G.; Liu, B. Hierarchical Fe₂O₃ nanorods/TiO₂ nanosheets heterostructure: Growth mechanism, enhanced visible-light photocatalytic and photoelectrochemical performances. *Appl. Surf. Sci.* **2019**, *475*, 380–388. [[CrossRef](#)]
31. Banisharif, A.; Khodadadi, A.A.; Mortazavi, Y.; Anaraki Firooz, A.; Beheshtian, J.; Agah, S.; Menbari, S. Highly active Fe₂O₃-doped TiO₂ photocatalyst for degradation of trichloroethylene in air under UV and visible light irradiation: Experimental and computational studies. *Appl. Catal. B Environ.* **2015**, *165*, 209–221. [[CrossRef](#)]
32. Palanisamy, B.; Babu, C.M.; Sundaravel, B.; Anandan, S.; Murugesan, V. Sol–gel synthesis of mesoporous mixed Fe₂O₃/TiO₂ photocatalyst: Application for degradation of 4-chlorophenol. *J. Hazard. Mater.* **2013**, *252–253*, 233–242. [[CrossRef](#)] [[PubMed](#)]
33. Mchedlov-Petrosyan, N.O.; Vodolazkaya, N.A.; Doroshenko, A.O. Ionic Equilibria of Fluorophores in Organized Solutions: The Influence of Micellar Microenvironment on Protolytic and Photophysical Properties of Rhodamine B. *J. Fluoresc.* **2003**, *13*, 235–248. [[CrossRef](#)]
34. Baran, T.; Wojtyła, S.; Minguzzi, A.; Rondinini, S.; Vertova, A. Achieving efficient H₂O₂ production by a visible-light absorbing, highly stable photosensitized TiO₂. *Appl. Catal. B Environ.* **2019**, *244*, 303–312. [[CrossRef](#)]
35. Feilizadeh, M.; Attar, F.; Mahinpey, N. Hydrogen peroxide-assisted photocatalysis under solar light irradiation: Interpretation of interaction effects between an active photocatalyst and H₂O₂. *Can. J. Chem. Eng.* **2019**, *97*, 2009–2014. [[CrossRef](#)]
36. Castellanos, R.M.; Paulo Bassin, J.; Dezotti, M.; Boaventura, R.A.R.; Vilar, V.J.P. Tube-in-tube membrane reactor for heterogeneous TiO₂ photocatalysis with radial addition of H₂O₂. *Chem. Eng. J.* **2020**, *395*, 124998. [[CrossRef](#)]
37. Lachheb, H.; Puzenat, E.; Houas, A.; Ksibi, M.; Elaloui, E.; Guillard, C.; Herrmann, J.-M. Photocatalytic degradation of various types of dyes (Alizarin S, Crocein Orange G, Methyl Red, Congo Red, Methylene Blue) in water by UV-irradiated titania. *Appl. Catal. B Environ.* **2002**, *39*, 75–90. [[CrossRef](#)]
38. Chaudhuri, M.; Elmolla, E.S.; Othman, R.B. Removal of reactive dyes from aqueous solution by adsorption on coconut coir activated carbon. In Proceedings of the 2nd International Conference on Engineering Technology 2009 (ICET 2009), Kuala Lumpur, Malaysia, 8–10 December 2009.
39. Zheng, R.; Yang, D.; Chen, Y.; Bian, Z.; Li, H. Fe₂O₃/TiO₂/reduced graphene oxide-driven recycled visible-photocatalytic Fenton reactions to mineralize organic pollutants in a wide pH range. *J. Environ. Sci.* **2023**, *134*, 11–20. [[CrossRef](#)] [[PubMed](#)]
40. Trenczek-Zajac, A.; Synowiec, M.; Zakrzewska, K.; Zazakowny, K.; Kowalski, K.; Dziedzic, A.; Radecka, M. Scavenger-Supported Photocatalytic Evidence of an Extended Type I Electronic Structure of the TiO₂@Fe₂O₃ Interface. *ACS Appl. Mater. Interfaces* **2022**, *14*, 38255–38269. [[CrossRef](#)] [[PubMed](#)]
41. Sun, Y.; Pignatello, J.J. Evidence for a surface dual hole-radical mechanism in the titanium dioxide photocatalytic oxidation of 2,4-D. *Environ. Sci. Technol.* **1995**, *29*, 2065–2072. [[CrossRef](#)] [[PubMed](#)]
42. Maurino, V.; Minella, M.; Sordello, F.; Minero, C. A proof of the direct hole transfer in photocatalysis: The case of melamine. *Appl. Catal. A Gen.* **2016**, *521*, 57–67. [[CrossRef](#)]
43. Malika, M.; Sonawane, S.S. The sono-photocatalytic performance of a Fe₂O₃ coated TiO₂ based hybrid nanofluid under visible light via RSM. *Colloids Surf. A Physicochem. Eng. Asp.* **2022**, *641*, 128545. [[CrossRef](#)]
44. Arora, I.; Chawla, H.; Chandra, A.; Sagadevan, S.; Garg, S. Advances in the strategies for enhancing the photocatalytic activity of TiO₂: Conversion from UV-light active to visible-light active photocatalyst. *Inorg. Chem. Commun.* **2022**, *143*, 109700. [[CrossRef](#)]
45. Du, S.; Lian, J.; Zhang, F. Visible Light-Responsive N-Doped TiO₂ Photocatalysis: Synthesis, Characterizations, and Applications. *Trans. Tianjin Univ.* **2022**, *28*, 33–52. [[CrossRef](#)]

Disclaimer/Publisher’s Note: The statements, opinions and data contained in all publications are solely those of the individual author(s) and contributor(s) and not of MDPI and/or the editor(s). MDPI and/or the editor(s) disclaim responsibility for any injury to people or property resulting from any ideas, methods, instructions or products referred to in the content.